Transient-State Reduction and Steady-State Kinetic Studies of Menaquinol Oxidase from *Bacillus subtilis*, Cytochrome aa_3-600 nm. Spectroscopic Characterization of the Steady-State Species[†]

Neil R. Mattatall,[‡] Linda M. Cameron, and Bruce C. Hill*

Department of Biochemistry, Queen's University, Kingston, Ontario K7L 3N6, Canada

Received May 31, 2001; Revised Manuscript Received August 28, 2001

ABSTRACT: Cytochrome aa_3-600 or menaquinol oxidase, from *Bacillus subtilis*, is a member of the heme−copper oxidase family. Cytochrome aa_3-600 contains cytochrome *a*, cytochrome a_3, and Cu_B, and each is coordinated via histidine residues to subunit I. Subunit II of cytochrome aa_3-600 lacks Cu_A, which is a common feature of the cytochrome *c* oxidase family members. Anaerobic reduction of cytochrome aa_3-600 by the substrate analogue 2,3-dimethyl-1,4-naphthoquinone (DMN) resolves two distinct kinetic phases by stopped-flow, single-wavelength spectrometry. Global analysis of time-resolved, multiwavelength spectra shows that during these distinct phases cytochromes *a* and a_3 are both reduced. Cyanide binding to cytochrome a_3 enhances the fast phase rate, which in the presence of cyanide can be assigned to cytochrome *a* reduction, whereas cytochrome a_3-cyanide reduction is slow. The steady-state activity of cytochrome aa_3-600 exhibits saturation kinetics as a function of DMN concentration with a K_m of 300 μM and a maximal turnover of 63.5 s^{-1}. Global kinetic analysis of steady-state spectra reveals a species that is characteristic of a partially reduced oxygen adduct of cytochrome a_3-Cu_B, whereas cytochrome *a* remains oxidized. Electron paramagnetic resonance (EPR) spectroscopy of the oxidase in the steady state shows the expected signal from ferricytochrome *a*, and a new EPR signal at $g = 2.01$. A model of the catalytic cycle for cytochrome aa_3-600 proposes initial electron delivery from DMN to cytochrome *a*, followed by rapid heme to heme electron transfer, and suggests possible origins of the radical signal in the steady-state form of the enzyme.

The heme−copper oxidase family of integral membrane enzymes includes mitochondrial and bacterial cytochrome *c* oxidases and several bacterial quinol oxidases. Members of this enzyme family catalyze the reduction of dioxygen to water with electrons derived from the protein substrate cytochrome *c*, or from a lipid-soluble quinol (*1*). In addition, members of the heme−copper oxidase family use the free energy available from the redox reaction to generate an electrochemical gradient across the membrane in which they are resident. These oxidases share the physical feature of having a coupled, binuclear heme and copper center that functions in the binding, activation, and reduction of dioxygen (*2*, *3*). In mitochondrial cytochrome *c* oxidase, the binuclear center is composed of cytochrome a_3 and Cu_B, whereas in ubiquinol oxidase from *Escherichia coli* the O_2 reaction site has cytochrome o_3 and Cu_B. In menaquinol oxidase from *Bacillus subtilis*, the binuclear center is more analogous to the mitochondrial oxidase in that it uses heme A, along with Cu_B, in the O_2 reaction site. It is anticipated, therefore, that the spectral signatures of the cytochrome aa_3-600 complex will be closer to those states previously characterized for mitochondrial cytochrome *c* oxidase and will facilitate interpretation of kinetic processes.

The spectroscopic properties of menaquinol oxidase from *B. subtilis* have been characterized by a number of approaches. The enzyme has been given the name cytochrome aa_3-600 because of the presence of heme A in both cytochrome centers and to indicate the distinctive shift to 600 nm of the α-band absorption maximum from 605 nm seen with mitochondrial cytochrome *c* oxidase (*4*). The cytochrome a_3-Cu_B center has been found to resemble in many respects the oxygen reaction site found in mitochondrial cytochrome *c* oxidase. The cytochrome a_3 iron is closely coupled to Cu_B, as revealed by EXAFS[1] spectroscopy (*5*, *6*). The interaction of cytochrome a_3-Cu_B with ligands, such as cyanide (*7*) and hydrogen peroxide (*8*), shows reactivity similar to the mitochondrial enzyme. In addition, single-turnover studies of the reduced enzyme with the oxidative substrate, oxygen, reveal a reaction similar to other members of the cytochrome oxidase family (*9*). The reduced enzyme reacts rapidly with oxygen to form an oxygen adduct at cytochrome a_3, and this decays as electron transfer ensues from the cytochrome *a* center.

[†] This work was supported by operating grants from the Natural Sciences and Engineering Research Council (Canada) and the Canadian Institutes of Health Research to B.C.H.

* Corresponding author. Phone: (613) 533-6375. Fax: (613) 533-2497. E-mail: hillb@post.queensu.ca.

[‡] Present address: Institute for Marine Biosciences, National Research Council Canada, 1411 Oxford St., Halifax, Nova Scotia, Canada B3H 3Z1.

[1] Abbreviations: DMN, 2,3-dimethyl-1,4-naphthoquinone; EPR, electron paramagnetic resonance; EXAFS, extended X-ray absorption fine structure; SVD, singular value decomposition; 3-CP, 3-carboxy-PROXYL, 3-carboxy-2,2,5,5-tetramethyl-1-pyrrolidinyloxy.

10.1021/bi011116q CCC: $20.00
Published on Web 10/03/2001

Electron input and steady-state kinetics of the cytochrome aa_3-600 complex have not been thoroughly explored. Kröger and co-workers have shown the selectivity of the enzyme for naphthoquinone-based substrates, and in a series of menaquinol analogues, the steady-state activity is greater as the redox potential of the analogue becomes more reducing (*10*, *11*). In the cytochrome *c* oxidase reaction, electrons are delivered to the oxygen reaction site by a series of intermediate carriers (*12*). Electrons are passed from ferrocytochrome *c* to Cu_A and then onto cytochrome *a* from where they proceed to the binuclear center. The menaquinol oxidase from *B. subtilis* lacks the Cu_A center, and presumably electrons are passed from menaquinol directly to cytochrome *a* and then on to the binuclear center. A further exploration of this process is one of the motivations behind the present work.

We show here that transient reduction of cytochrome aa_3-600 in the absence of oxygen proceeds in two kinetic phases and that reduction of both cytochrome centers occurs in both phases. In the presence of cyanide, reduction of cytochrome a_3 still proceeds, but slowly, and the apparent rate and extent of cytochrome *a* reduction are increased relative to its reduction in the ligand-free enzyme. In steady-state studies, cytochrome aa_3-600 exhibits saturation kinetics as a function of DMN concentration. Optical spectroscopy of the steady-state reaction reveals little reduction of cytochrome *a* and the presence of an oxygen adduct of cytochrome a_3. The EPR spectrum of cytochrome aa_3-600 frozen in the steady state shows that cytochrome *a* remains oxidized and reveals a new species at $g = 2.01$. When the steady-state sample is thawed, the enzyme continues turnover activity, leading to complete oxygen consumption and reduction of the enzyme. At this point, the low-spin heme signal from ferricytochrome *a* and the $g = 2.01$ signal disappear. These data imply that in the steady-state reaction and transient-state reduction of cytochrome aa_3-600, intramolecular electron transfer occurs much faster than electron input from menaquinol. A model is presented in which initial electron input is to cytochrome *a* from menaquinol, and this is followed by rapid electron transfer from cytochrome *a* to the binuclear center, which occurs even in the absence of oxygen. In the steady-state reaction, reduction of cytochrome a_3-Cu_B is followed by rapid reaction with O_2 to form an intermediate complex with an altered ligand-bound state of cytochrome a_3.

MATERIALS AND METHODS

Cytochrome aa_3-600 was purified from *B. subtilis* as described previously (*13*) except that the initial hydroxyapatite column was replaced by a column of Fast Flow Chelating-Sepharose (Pharmacia, Montreal, PQ) equilibrated with nickel. DMN was purchased from St.Sava-Bioanalyt. & Med. Research (Kingston, ON) and was prepared as a 50 mM stock solution in ethanol. Lauryl maltoside was from Anatrace (Maumee, OH). D,T-Diaphorase, reduced nicotinamide adenine dinucleotide, and 3-CP were purchased from Sigma (Oakville, ON) and stock solutions made just prior to use. All other chemicals and reagents were of the highest quality commercially available.

Steady-State Assay and Analysis. Spectrophotometric assays of cytochrome aa_3-600 activity were done using a Hewlett-Packard diode array. The assay system contained oxidized cytochrome aa_3-600 at a concentration of 2−5 μM in phosphate buffer, pH 6.5, containing 0.5 mg/mL lauryl maltoside. Two millimolar NADH and 2 mg/mL diaphorase were added just prior to the start of the assay which was initiated by addition of DMN. The concentrations of NADH and diaphorase used were determined to be saturating in separate experiments. The time taken for complete consumption of dissolved dioxygen (i.e., anaerobiosis time or t_{an}) was indicated when the enzyme suddenly increased in reduction from the steady state. Anaerobiosis times were used to determine molecular activity as follows:

$$v(\mu\text{equiv/s}) = ([O_2](\mu\text{M}) \times 4)/t_{an}(\text{s})$$

$$\text{TN}(\text{s}^{-1}) = v/[aa_3](\mu\text{M})$$

where v is the velocity in electrons per second, the dissolved O_2 concentration in air-equilibrated buffer is calculated as 240 μM, and the concentration of the cytochrome aa_3 complex is determined from the reduced minus oxidized difference spectrum using an extinction coefficient of 26 mM^{-1} cm^{-1} at 600−630 nm (*4*).

Steady-state and anaerobic reduction time courses were the subject of global analysis using the program Specfit/32 (Spectrum Software Associates, Chapel Hill, NC). This involves an initial singular value decomposition of the three-dimensional data set. A set of kinetic models were then supplied and a least-squares fit made to the data. The models that are presented gave the best fit to the data after several iterations of adjusting the magnitude of the observed rate constants and allowing the program to find the best global solution.

Stopped-Flow Reduction. Reduction time courses using concentrations of DMN above 5 μM required rapid mixing, and a Durrum-Gibson stopped-flow spectrometer was used. The stopped-flow device was made anaerobic by first rinsing with argon-equilibrated buffer, followed by an incubation with anaerobically prepared 2 mM sodium dithionite and then removing dithionite by rinsing with argon-equilibrated buffer. The instrument and data collection were under the control of OLIS (Athens, GA) software. Pseudo-first-order rate constants and absorbance magnitudes were extracted from these data by fitting to the appropriate kinetic model using Specfit/32. Stock dithionite concentrations were prepared for these experiments in argon-equilibrated buffer.

EPR Spectroscopy of Steady-State Cytochrome aa_3. EPR spectra were obtained on a Bruker EMX spectrometer at X-band fitted with an HSQ (Bruker Canada, Milton, ON) cavity and liquid helium flow cryostat (Oxford Instruments, U.K.) for temperature control. The standard instrument conditions were as follows: $T = 10$ K, modulation amplitude = 20 G, power = 2 mW at a gain of 1×10^4. In experiments done to look at the radical line shape, the modulation amplitude was reduced to 2 G. The enzyme for EPR experiments was present in the range of 20−40 μM and was brought into the steady state by addition of 2 mM NADH, 1−2 mg/mL D,T-diaphorase, and 50 μM DMN to an aerated solution in a 2 mm cuvette. Time-resolved absorption spectra were measured to determine the steady-state optical spectrum of the sample prior to its transfer into an EPR tube, which was then submerged in a bath of ethanol maintained at low temperature over a pool of liquid N_2. The frozen sample was then placed directly into liquid N_2 prior to transfer to the

flow cryostat. Following the EPR spectral assessment, the sample was thawed and returned to the diode-array spectrometer where the steady-state reaction was allowed to proceed to anaerobiosis and full reduction, whereupon the sample was again frozen rapidly and returned to the EPR cryostat for spectral assessment. Quantification of the free radical signal was performed by determining the intensity through double integration and comparing that to the intensity of the stable free radical 3-carboxy-PROXYL measured under nonsaturating conditions.

RESULTS

Anaerobic Reduction of Oxidized and Oxidized, Cyanide-Bound Cytochrome aa_3-600 by Reduced DMN Using Stopped-Flow Mixing and Single-Wavelength Detection. Sodium dithionite is not an effective reductant of cytochrome aa_3-600, presumably due to lack of the Cu_A center. We have taken advantage of this property to use dithionite as a reductant of the substrate analogue DMN, and to facilitate the study of this reaction using strict anaerobic conditions. The following scheme describes the overall reduction of menaquinol oxidase by sodium dithionite plus DMN:

$$1.5S_2O_4^{2-} + 1.5\text{DMN} + 3H^+ \rightarrow 1.5\text{DMNH}_2 \quad (1)$$

$$1.5\text{DMNH}_2 + aa_3(\text{ox}) \rightarrow 1.5\text{DMN} + aa_3(\text{red}) + 3H^+ \quad (2)$$

where the oxidized and reduced forms of cytochrome aa_3-600 are indicated as aa_3(ox) and aa_3(red), respectively. The kinetics of reduction of cytochrome aa_3-600 were monitored at 444 nm following stopped-flow mixing at a series of DMN concentrations (Figure 1). The time course of reduction by dithionite alone is fit by a single-exponential process with an observed rate of 0.0104 ± 0.0012 s^{-1} at 1 mM sodium dithionite (Figure 1A). When DMN is included with dithionite, the overall reaction is much faster, and there are two kinetic phases resolved. At a DMN concentration of 5.5 μM illustrated in panel B, the rates are 5.34 ± 0.15 s^{-1} for the fast phase and 0.097 ± 0.015 s^{-1} for the slow phase. Both the fast and slow phase rates increase with increasing DMN concentration (Figure 2). The fast phase exhibits a hyperbolic dependence upon DMN concentration. At concentrations below 20 μM, the fast phase rate is proportional to DMN concentration and corresponds to a second-order rate of 1×10^6 M^{-1} s^{-1}. The observed rate reaches a limit of about 80 s^{-1} above 300 μM DMN. The slow phase rate is proportional to DMN concentration over the entire range studied here with a second-order rate of 2.1×10^4 M^{-1} s^{-1}.

Cytochrome aa_3-600 binds cyanide to form a complex that results in a low-spin state of cytochrome a_3 which remains bridged to and magnetically interacting with Cu_B (*7*). The effect of cyanide binding on the reactivity of cytochrome aa_3-600 is to accelerate the rate of the fast phase and to slow the rate of the second phase of reduction. Table 1 compares the observed rates and extents for the fast and slow phases at two different DMN concentrations for the same sample of cytochrome aa_3-600 in unliganded and cyanide-bound states. The magnitudes of the fast phase rate double in the presence of cyanide and remain dependent upon DMN concentration. In contrast, the second phase is slower in the presence of cyanide, and the rate is almost independent from

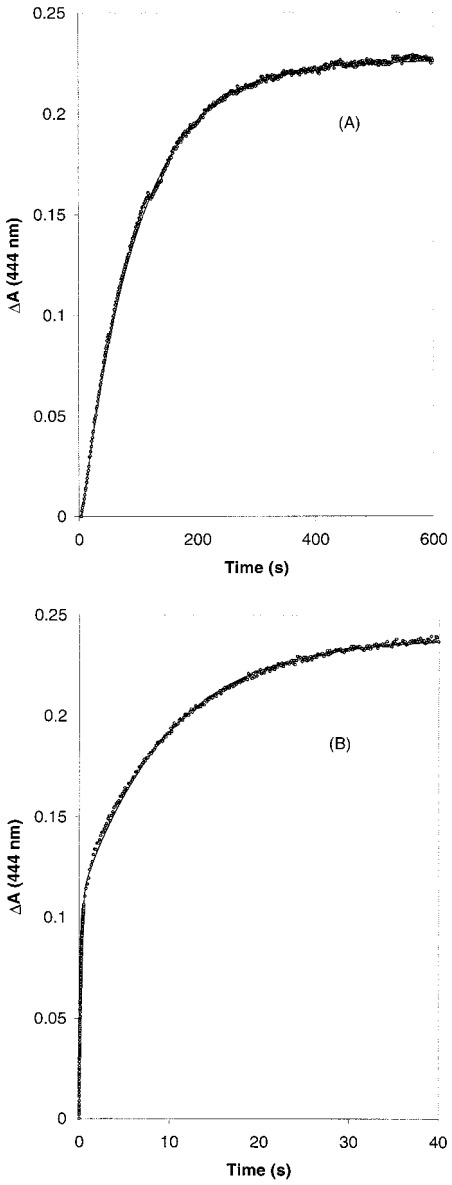

FIGURE 1: Anaerobic reduction of cytochrome aa_3-600. (A) Reduction by dithionite alone. The reaction time course was monitored at 444 nm following stopped-flow mixing of argon-equilibrated cytochrome aa_3-600 with sodium dithionite. The final concentration of enzyme was 2 μM, and sodium dithionite concentration was 1 mM. The buffer was 100 mM sodium phosphate, pH 6.5, with 0.5 mg/mL lauryl maltoside. The smooth line through the data is a single-exponential fit. (B) Reduction by dithionite plus DMN. The conditions were the same as in panel A except that DMN was present in the dithionite-containing syringe of the stopped-flow. The final DMN concentration was 5.5 μM. Data were collected on the same sample at two different rates to span the entire time range. The smooth line through the data is a double-exponential fit.

DMN concentration. The extents of the fast and slow phases are similar in magnitude except for cyanide-bound oxidase with low DMN. In this situation, complete reduction of cytochrome a_3-CN is not achieved.

Diode-Array Detection and Multiwavelength Analysis of Anaerobic Reduction of Cytochrome aa_3-600 by Dithionite plus DMN. To determine the spectral characteristics of the kinetic components resolved in the stopped-flow experiments above, the reduction process was studied at an appropriate DMN concentration using multiwavelength detection. Figure

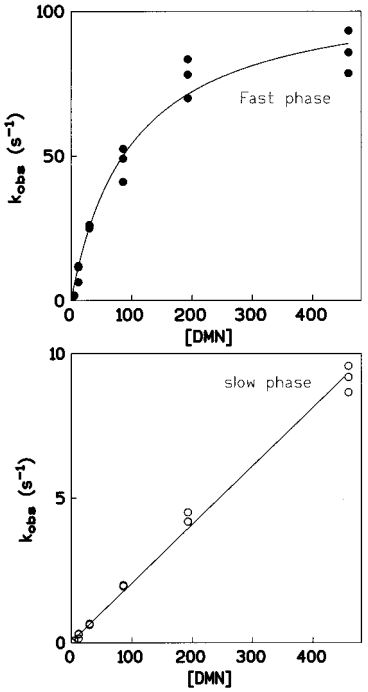

FIGURE 2: Concentration dependence of the observed rate of cytochrome aa_3-600 reduction by DMN. (A) Rate of the fast phase as a function of DMN concentration. The values derived from three independent stopped-flow measurements are shown at each concentration of DMN. (B) Rate of the slow phase as a function of DMN concentration. The conditions for the experiment are identical to those described in the legend to Figure 1.

3 shows time-resolved UV−visible difference spectra from 380 to 700 nm, obtained with a diode-array spectrometer, when sodium dithionite plus DMN is added to argon-equilibrated, oxidized cytochrome aa_3-600. The spectrum of the oxidized enzyme has been subtracted as the reference state for each spectrum. The three-dimensional data set was subjected to singular-value decomposition and global kinetic analysis according to the following reaction scheme:

$$aa_3(\text{ox}) + \text{DMN(red)} \rightarrow aa_3(\text{pr}) + \text{DMN(ox)} \quad (3)$$

$$aa_3(\text{pr}) + \text{DMN(red)} \rightarrow aa_3(\text{red}) + \text{DMN(ox)} \quad (4)$$

$$aa_3(\text{red}) \rightarrow aa_3(\text{red})' \quad (5)$$

$$c(\text{ox}) + \text{DMN(red)} \rightarrow c(\text{red}) + \text{DMN(ox)} \quad (6)$$

where aa_3(ox) is oxidized enzyme, DMN(red) is reduced DMN, DMN(ox) is oxidized DMN, aa_3(pr) is partially reduced menaquinol oxidase, and aa_3(red) and aa_3(red)′ are two forms of fully reduced menaquinol oxidase. The kinetic conditions are pseudo-first-order because the reduced DMN concentration is unchanged throughout the course of the reaction due to the presence of dithionite.

The species *c*(ox) and *c*(red) refer to the oxidized and reduced forms, respectively, of a small amount of a contaminating species of *c*-type cytochrome, as judged by its absorption spectrum. In this preparation, the *c*-type cytochrome is present at a level of 10% relative to the oxidase, and a component had to be added to the kinetic scheme to produce a global fit to the observed data. The presence of this contaminating cytochrome varies from nondetectable to 10% in experiments performed with different preparations of cytochrome aa_3-600. Its presence does not affect the observed reduction kinetics of cytochrome aa_3-600, presumably because cytochrome aa_3-600 does not use cytochrome *c* as a substrate (*4*, *13*).

The kinetic model describes three reaction components associated with reduction of cytochrome aa_3-600. The pseudo-first-order rates for the fastest to slowest phase are 0.57, 0.097, and 0.011 s^{-1}, corresponding to eqs 3, 4, and 5 above. Figure 3B shows the spectra of these three forms of menaquinol oxidase, and they are similar to one another with minima at 416 nm and maxima at 444 and 600 nm. An extra component of intermediate rate is resolved in the multiwavelength experiments that was not required to produce a satisfactory fit to the data from the single-wavelength, stopped-flow experiments. Failure to resolve the intermediate phase with single-wavelength detection is presumably because of the relatively small difference in rate between the fast and intermediate phases, the small absorbance contribution of the intermediate component, and the fact that the fast and slow phase contributions at 444 nm are both positive. The resolution of an intermediate phase in the multiwavelength data set is an example of the improvement in kinetic resolution achieved when SVD and global analysis are applied. The magnitude of the fastest phase component [i.e., aa_3(pr) in eq 3] contributes 62% to the overall absorption at 444 nm and only 42% to the intensity at 600 nm. Such spectral and kinetic features cannot be assigned to a process in which the initial phase is due to reduction of cytochrome *a* alone, and the second phase due to cytochrome a_3 reduction, as can be done for the two-phase reaction of bovine heart cytochrome *c* oxidase with dithionite (*14*). In contrast, the findings with cytochrome aa_3-600 are consistent with partial reduction of both cytochrome *a* and cytochrome a_3 during each stage of the reaction. Such a model implies rapid electron exchange between the two heme centers in the partially reduced enzyme.

As shown above, reduction of oxidized, cyanide-bound cytochrome aa_3-600 is also a complex kinetic process. A multiwavelength data set for reduction of cyanide-bound cytochrome aa_3-600 nm is shown in Figure 4. This experiment was performed with the same sample at the same enzyme concentration as the multiwavelength set displayed above for reduction of oxidized, unliganded enzyme. The data are fit best with three components representing reduction of cytochrome aa_3-600 and two components for reduction of contaminating *c*-type cytochrome. The extra kinetic component is to account for the slow reduction induced by the binding of cyanide to the contaminating cytochrome *c*. The absorption spectra for the oxidase components resolved from the kinetic model are shown in panel B.

Figure 5 compares time-resolved difference spectra for the reduction of unliganded enzyme and cyanide-bound enzyme. These spectra are derived from the spectra shown in Figures 3B and 4B. The difference spectra of the initial fast component minus oxidized for each case are compared in panel A. The fast component for the enzyme with cyanide bound to cytochrome a_3 shows features characteristic for reduction of cytochrome *a*: an intense sharp α-band at 600 nm, a Soret peak at 446 nm with a long-wavelength shoulder at 450 nm, and a trough at 426 nm. These features have also been observed in assigning the spectrum of cytochrome *a* in a ligand binding approach with cytochrome aa_3-600 (*7*) and for mitochondrial oxidase (*7*, *15*), and are also similar

Table 1: Rates of Reduction [k_{obs} (s^{-1})] and Magnitudes of Absorbance Change (ΔA) in the Reaction of Cytochrome aa_3-600 with Dithionite plus DMN[a]

	unliganded				cyanide-bound			
	fast		slow		fast		slow	
[DMN] (μM)	k_{obs} (s^{-1})	ΔA	k_{obs} (s^{-1})	ΔA	k_{obs} (s^{-1})	ΔA	k_{obs} (s^{-1})	ΔA
2.5	2.59 ±0.21	0.113 ±0.0063	0.0475 ±0.0032	0.120 ±0.0084	4.93 ±0.34	0.124 ±0.0032	0.0224 ±0.0078	0.068 ±0.0091
59	25.1 ±5.80	0.098 ±0.0072	2.07 ±0.58	0.106 ±0.0072	47.2 ±5.4	0.119 ±0.0064	0.0847 ±0.0057	0.118 ±0.0156

[a] Observed rates have been extracted from individual time courses measured at 444 nm by fitting the reaction to a double-exponential equation. Each value is the average of at least three measurements from which the mean and standard deviation were calculated. The enzyme concentration in each case was 2.0 μM, and the buffer was 100 mM sodium phosphate, pH 6.5, with 0.5 mg/mL lauryl maltoside. The temperature was 20 °C. The cyanide-bound enzyme was prepared just prior to the experiment by incubation of the oxidized, unliganded enzyme for 40 min. The final cyanide concentration was 5 mM.

to the spectral-kinetic form assigned to cytochrome *a* for mitochondrial oxidase (*14*). In contrast, the spectrum for the rapidly reduced species in the absence of cyanide has a weaker, broader α-band accompanied by an intense Soret band. These features are consistent with the simultaneous reduction of both cytochrome *a* and a_3 centers. Spectra of the slowest developing components are compared in panel B. These spectra were generated by taking a difference between the final spectrum minus the intermediate phase spectrum. In the absence of cyanide, the spectral form is consistent with a contribution from both cytochromes, whereas the shift of the α-band to 595 nm in the presence of cyanide is indicative of the formation of ferrocytochrome a_3-CN.

Steady-State Kinetics of Cytochrome aa_3-600 Using Reduced DMN as Substrate. Figure 6 shows a schematic outline of the coupled assay used to measure the steady-state activity of menaquinol oxidase. NADH is used as the ultimate source of reducing equivalents to drive the eventual reduction of oxygen to water. The passage of electrons from NADH to DMN is catalyzed by D,T-diaphorase. The reduction of quinones by D,T-diaphorase is known to proceed by a two-electron, hydride-transfer mechanism (*16*).

A comparison of a series of naphthoquinone derivatives found DMN to exhibit the highest activity (*10*). However, a systematic study of the dependence of menaquinol oxidase activity upon substrate concentration has not been reported. A set of traces recorded at 444−460 nm from the spectrophotometric assay of menaquinol oxidase is shown in Figure 7A. At time zero, the enzyme is fully oxidized, and the reaction is started by addition of NADH, diaphorase, and DMN. The absorbance moves to a steady level immediately, and this is maintained until oxygen is completely exhausted. The enzyme then proceeds to the fully reduced state as indicated by the sharp increase in absorbance at 444−460 nm. The time spent in the steady state is dependent on the DMN concentration, and this can be used to construct a plot of velocity versus DMN concentration (Figure 7B). In addition, when oxygen is stirred into the cuvette, the enzyme immediately returns to the level of absorbance observed in the previous steady state and then returns shortly to the fully reduced state (data not shown). There is no apparent "resting to pulsed" type of activation phenomenon as observed when the analogous assay is performed with mitochondrial cytochrome *c* oxidase (*17*).

The assay was repeated at distinct DMN concentrations, and the activity was calculated from the anaerobiosis times as outlined under Materials and Methods. A plot of the apparent turnover as a function of DMN is hyperbolic, and an Eadie−Hofstee transformation is linear (Figure 7B, inset). The K_M for DMN is 300 μM, and the maximal turnover is 65 s^{-1}. However, it must be pointed out that the saturation behavior exhibited may be a reflection of the intolerance of the enzyme to ethanol or to limiting DMN solubility rather than an intrinsic catalytic limitation of cytochrome aa_3-600.

Global Analysis of Steady-State Assay. We have recorded spectra of menaquinol oxidase during steady-state activity at wavelengths over the Soret and visible regions using a diode-array spectrometer. A multiwavelength data set is shown in a three-dimensional presentation of absorbance versus wavelength, versus time (Figure 8A). This data set was subjected to singular-value decomposition to determine the basis spectra, and a kinetic model of the following form was used to fit the data:

$$DMNH_2 + \text{oxidized enzyme} \xrightarrow[k_1]{} DMN + \text{partially reduced enzyme} \quad (7)$$

$$\text{partially reduced enzyme} + O_2 \xrightarrow[k_2]{} \text{steady-state form} + H_2O \quad (8)$$

$$\text{steady-state form} + DMNH_2 \xrightarrow[k_3]{} DMN + \text{oxidized enzyme} + H_2O \quad (9)$$

$$\text{partially reduced enzyme} + DMNH_2 \xrightarrow[k_4]{} \text{fully reduced enzyme} \quad (10)$$

$$\text{fully reduced enzyme} \xrightarrow[k_5]{} \text{fully reduced enzyme}' \quad (11)$$

The reaction starts off with cytochrome aa_3-600 oxidized, and the enzyme is brought into the steady state by reaction with reduced DMN (reaction 7). This generates a partially reduced form of cytochrome aa_3-600 that is reactive with oxygen. This process is undoubtedly more complicated than that described by a single-step reaction, but we do not resolve any other intermediate partially reduced forms. The product of the reaction of partially reduced enzyme with O_2 is the steady-state form of the enzyme. The steady-state form can accept electrons from reduced DMN, presumably via ferricytochrome *a*, regenerating the oxidized enzyme that in turn accepts electrons to return to the oxygen-reactive, partially reduced state. It is the cycling between reactions 7, 8, and 9 that makes up the steady-state cycle. The fully reduced species is not required as a participant in the steady state in

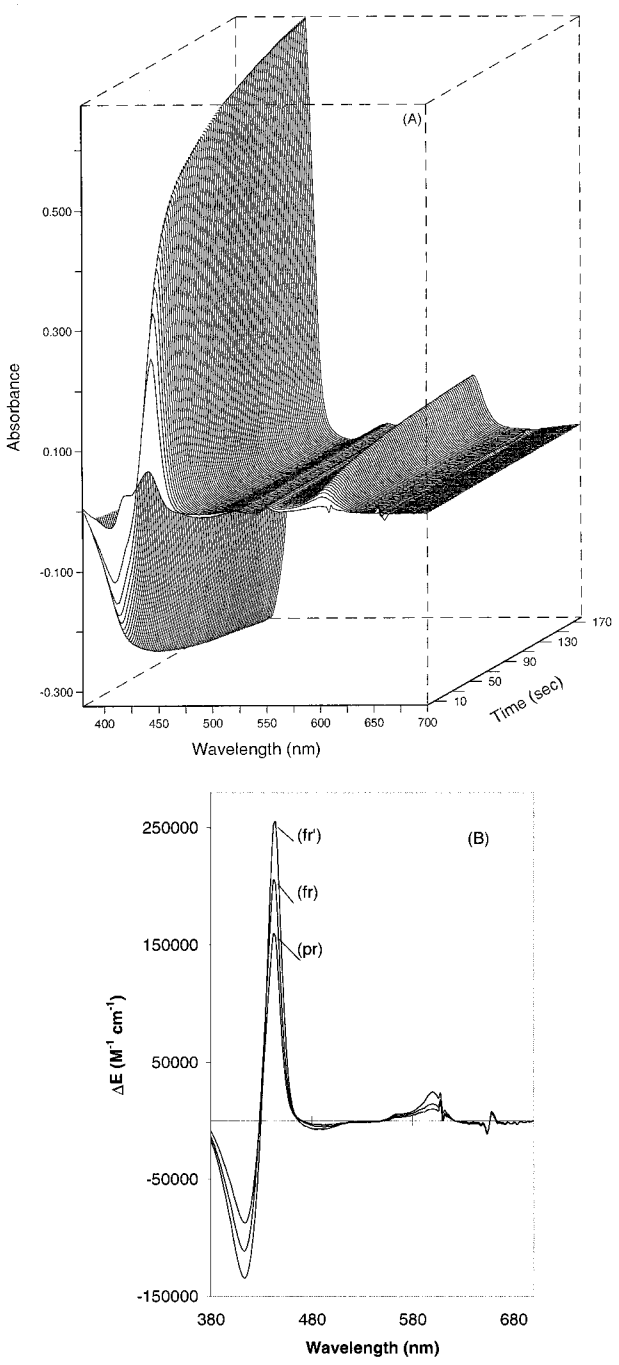

FIGURE 3: (A) Multiwavelength absorption changes during the anaerobic reduction of cytochrome aa_3. The enzyme concentration was 3.3 μM, and the reduction reaction was initiated by the addition 1 mM sodium dithionite plus 0.65 μM DMN. The enzyme and reductant solutions were equilibrated with argon prior to mixing. The buffer was 100 mM sodium phosphate, pH 6.5, with 0.5 mg/mL lauryl maltoside, and the temperature was 20 °C. Spectra were collected every 2 s for a total of 180 s. (B) Absorption spectra of the species of cytochrome aa_3-600 specified by the kinetic model outlined in the text. The spectra are shown on an intensity scale of molar extinction coefficient and are labeled as (pr), (fr), and (fr′) in order of increasing intensity and corresponding to partially reduced and fully reduced forms of the enzyme.

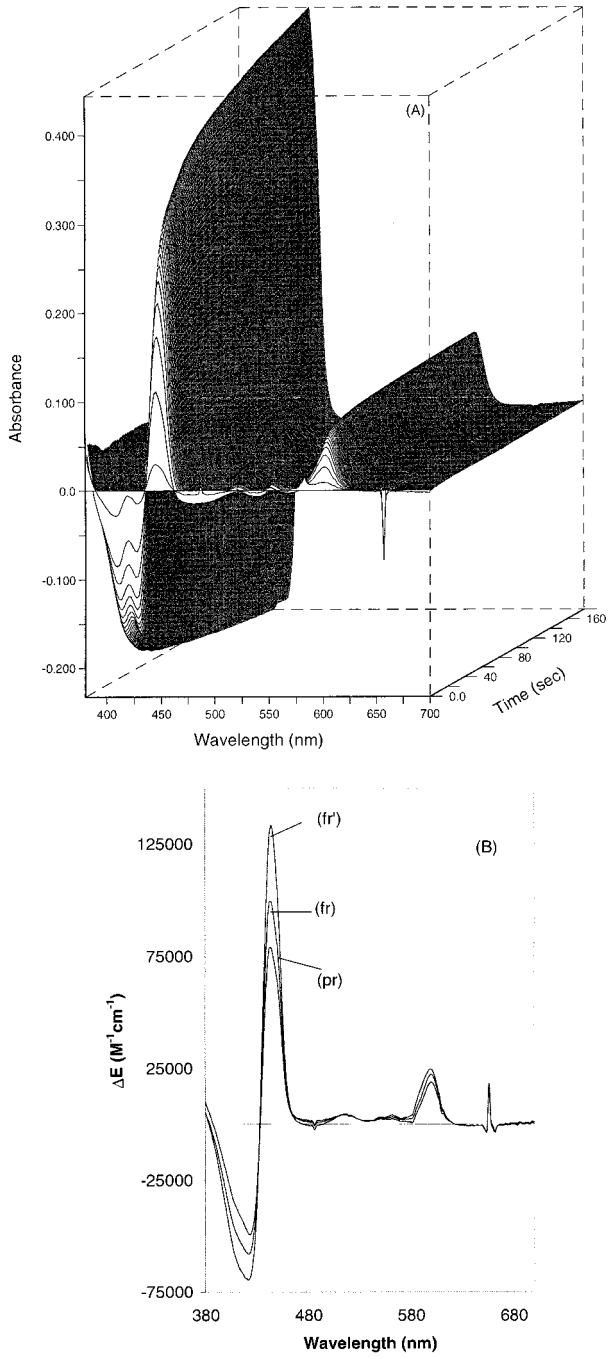

FIGURE 4: (A) Multiwavelength changes during the anaerobic reduction of cyanide-bound cytochrome aa_3-600. The conditions for this experiment were the same as outlined in the legend to Figure 3 except that the oxidized enzyme was incubated with 5 mM KCN for 1 h prior to the addition of the reductants. (B) Absorption spectra of the species of cytochrome aa_3-600 specified by the kinetic model outlined in the text. The spectra are shown on an intensity scale of molar extinction coefficient and are labeled as (pr), (fr), and (fr′) in order of increasing intensity and corresponding to partially reduced and fully reduced forms of the enzyme.

the model outlined here. When the oxygen is exhausted, reaction 8 is blocked, and reaction 10 takes the enzyme to the fully reduced state. The rate constants used to produce the fit to the observed data are as follows: $k_1 = 2 \times 10^6$ M^{-1} s^{-1}, $k_2 = 5 \times 10^7$ M^{-1} s^{-1}, $k_3 = 3.7 \times 10^4$ M^{-1} s^{-1}, and $k_4 = 2.4 \times 10^3$ M^{-1} s^{-1}. This gives a generally satisfactory fit to the data, except that after the oxygen runs out there is an additional, slower kinetic step (i.e., reaction 11, $k_5 = 0.12$ s^{-1}) as the enzyme approaches full reduction. An example of the fit to the data from this model is illustrated for a single wavelength (Figure 9). The spectral forms of the enzyme generated from this fit are shown in Figure 8B,C. The spectral forms of the fully reduced and partially reduced

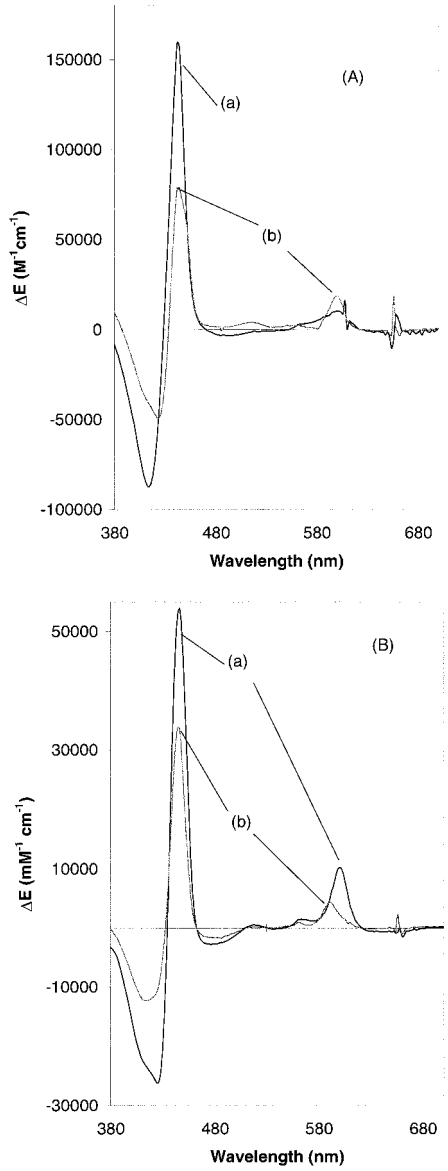

FIGURE 5: Comparison of time-resolved spectra from the anaerobic reduction of unliganded and cyanide-bound, oxidized cytochrome aa_3-600. (A) Basis spectra from the initial fast reduction of (a) unliganded enzyme and (b) cyanide-bound enzyme. These spectra are the same as those in Figures 3B and 4B labeled (pr). (B) Difference between the slow and intermediate rate spectra for (a) unliganded and (b) cyanide-bound enzyme. These spectra are constructed from data in Figures 3B and 4B (fr′ − fr).

states have Soret bands at 444 nm and a visible absorption at 600 nm that are both hallmarks of the reduced minus oxidized difference spectrum. In contrast, the steady-state species has absorption at 438 and 604 nm. These features have been previously observed and ascribed to the peroxy or P-state of cytochrome a_3 (*8*). In addition, the simulation specifies that better than 90% of the enzyme is in the P-state during turnover. The modeling yields spectra of the intermediate forms and extinction coefficients for the P intermediate minus oxidized (e.g., $\Delta E^{604-630} = 7.4$ mM^{-1} cm^{-1}) that are in reasonable agreement with the reported values from the bovine enzyme for this species (*18*).

Electron Paramagnetic Resonance Analysis of the Steady-State Form of Cytochrome aa_3-600. The UV−visible spectral properties of cytochrome aa_3-600 recorded in the steady-state indicate an oxygen adduct of cytochrome a_3 and

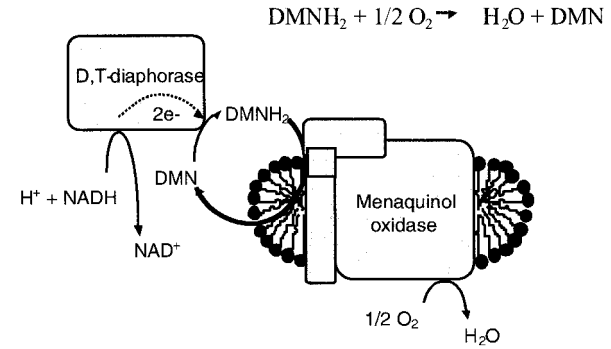

FIGURE 6: Scheme for the steady-state assay of cytochrome aa_3-600. The menaquinol oxidase or cytochrome aa_3-600 is shown as a three-subunit complex in a micelle of detergent. DMN is reduced to $DMNH_2$ by D,T-diaphorase at the expense of NADH.

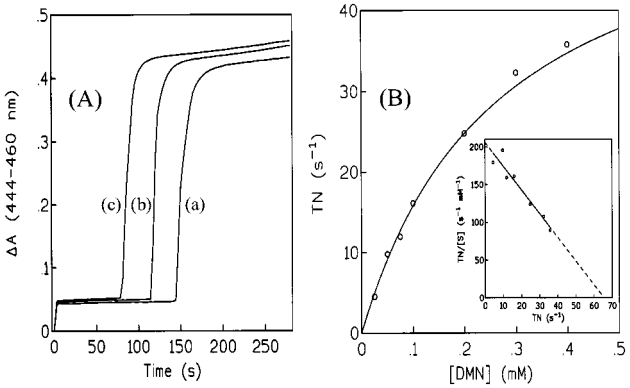

FIGURE 7: Steady-state activity assays of cytochrome aa_3-600. (A) Absorbance at 444 minus 460 nm is shown as a function of time at three different concentrations of DMN. Assays were carried out at 20 °C in a buffer of 50 mM sodium phosphate, pH 6.5, with 0.5 mg/mL lauryl maltoside and 2.4 μM cytochrome aa_3-600. The concentration of NADH was 2 mM, and the diaphorase was present at 2 mg/mL. Traces (a), (b), and (c) contained 25, 50, and 100 μM DMN, respectively. (B) Anaerobiosis times obtained from experiments such as those in panel A were converted to molecular activity and are plotted against DMN concentration. The smooth line through the data is a fit to a rectangular hyperbola using the values for K_M and TN_{max} mentioned in the text. The inset to panel B shows the Eadie−Hofstee transformation of the same data.

oxidized cytochrome *a*. In an effort to further define this intermediate state, we sought to measure its EPR spectrum. The enzyme was prepared in the same manner as described for optical spectral analysis. At the points indicated by the arrows on the time course of Figure 9, the sample was removed from the optical cuvette, transferred to an EPR tube, and immediately immersed in an ultra-cold ethanol bath. EPR spectra obtained for oxidized, steady-state, and reduced cytochrome aa_3-600 are shown in Figure 10A. The oxidized enzyme has a set of resonances at $g = 3.05$, 2.21, and 1.40 due to a low-spin heme center which have been assigned previously to cytochrome *a* (*4*). In the steady state, the low-spin heme spectral features and intensity are largely unchanged. This is consistent with our optical spectral data in which reduction of cytochrome *a* is minimal in the steady state. In addition, there is a small amount of signal from a high-spin heme center at each stage of the reaction. A new signal appears in the steady state that is centered at $g = 2.01$ (Figure 10B). This signal is isotropic in shape with a peak to peak width of 28 G. Power dependence studies from 2 μW to 50 mW reveal only a small degree of saturation over

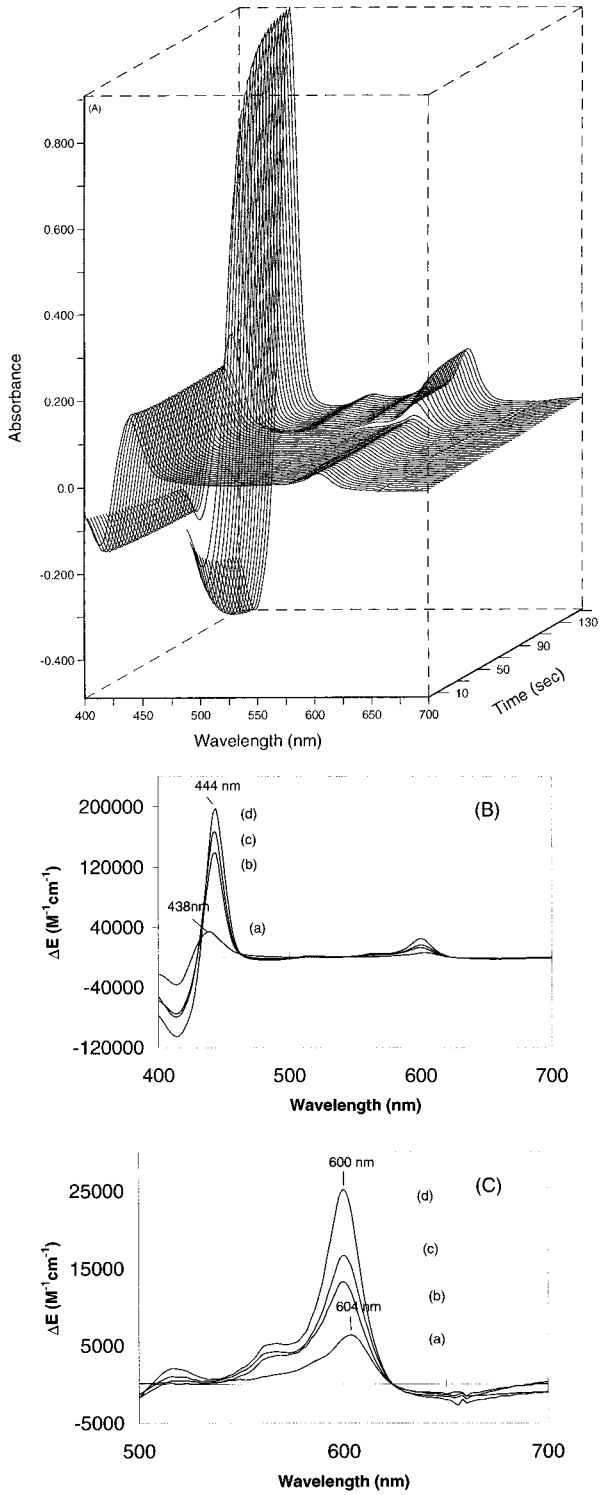

FIGURE 8: Multiwavelength assay of the steady-state activity of cytochrome aa_3-600. The cytochrome aa_3-600 concentration was 4.2 μM, and the DMN concentration was 50 μM. The other conditions in the assay were the same as those detailed in the legend to Figure 7. (A) Three-dimensional plot of the absorbance spectra collected as a function of time. (B) Basis spectra derived from the analysis of the data in panel (A). Trace (a) is of the steady-state species, (b) is the initially, partially reduced, oxygen-reactive form, (c) is the initial fully reduced species, and (d) is the final fully reduced spectrum. (C) Visible region of panel B shown on an expanded scale.

this range at 10 K. The spin intensity of the radical signal was determined by double integration against a known concentration of the stable free radical 3-carboxy-PROXYL

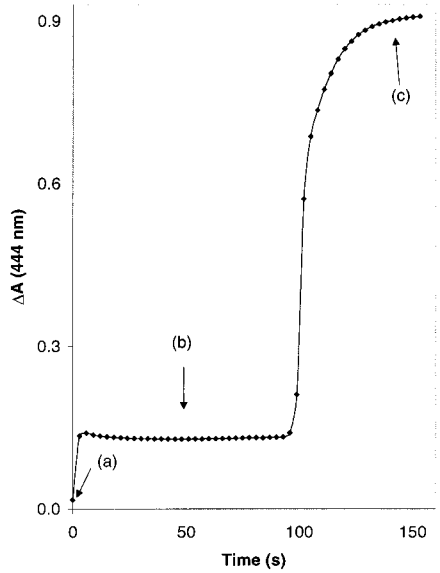

FIGURE 9: Single-wavelength trace and fit of the steady-state assay of cytochrome aa_3-600. The absorbance reading at 444 nm as a function of time has been extracted from the multiwavelength data set in Figure 8. The solid line through the data is drawn from the model outlined in the text. The points on the time course indicate when samples of (a) oxidized, (b) steady-state, and (c) reduced enzyme were removed for the EPR analysis shown in Figure 10.

measured under nonsaturating conditions. The radical signal amounted to 60% of 1 spin equiv, relative to the cytochrome aa_3-600 concentration. When the steady-state sample was thawed rapidly and returned to the optical spectrometer, the same absorption spectrum, as prior to rapid freezing, was observed. Further incubation of this sample at 20 °C led to transition from the steady state to full reduction upon depletion of dissolved oxygen. This sample was frozen rapidly again and returned to the EPR spectrometer. The signals associated with the low-spin heme and the radical center seen in the steady state were absent following anaerobiosis (Figure 10A, trace c). A spectrum of the steady-state species minus the fully oxidized enzyme is shown in panel B of Figure 10.

DISCUSSION

The form that an enzyme takes in the steady state is an important definition of its molecular activity as a catalyst. There are few enzyme systems for which the steady-state form has been well-defined. An initial, and continuing, appeal of heme-based and metal-based enzymes is the spectroscopic window afforded by the prosthetic group(s) to the microscopic details of catalysis. The heme−copper oxidase family of enzymes has attracted considerable attention, both in efforts to define its catalytic cycle and also as a prerequisite for understanding the process of energy coupling. Kinetic studies have focused on the redox partial reactions. These have included transient reduction studies of the oxidized enzyme and, more intensively, the oxygen reaction of both half-reduced (*19*) and fully reduced forms of the oxidase (*20*). Studies of the oxidative half-reaction have been particularly informative because the individual reaction steps are all catalytically competent in that they occur at, or well above, the known molecular turnover rate of the enzyme (*21*). The work here is aimed at defining the reductive-kinetic and steady-state properties of a member of the heme−copper

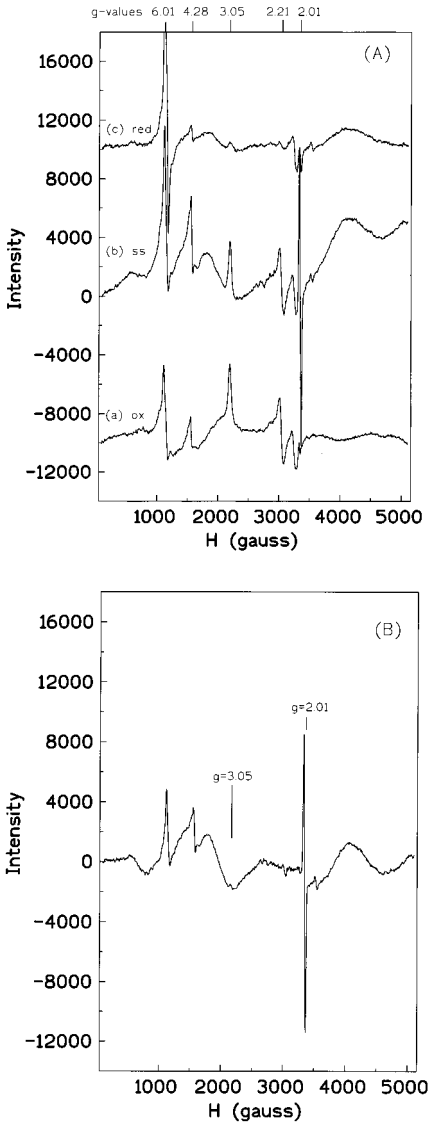

FIGURE 10: EPR spectra of cytochrome aa_3-600 during the steady-state activity assay. Panel A shows three spectra of the oxidase that were prepared by rapid freezing of a steady-state sample at the time points indicated on the time course in Figure 9: (a) before reductant addition, (b) during the steady state, and (c) after anaerobiosis. Panel B is an EPR difference spectrum between the steady-state form and the oxidized enzyme.

family of cytochrome oxidases, cytochrome aa_3-600 from the highly aerobic bacterium *B. subtilis*.

The kinetic model presented in Figure 11 can accommodate the transient-kinetic and steady-state experiments reported here. Reduction of the oxidized enzyme from reduced DMN begins with electron donation to cytochrome *a*, a reaction that is a bimolecular process with a second-order rate constant, as measured here, of 2×10^6 M^{-1} s^{-1}. Reduced cytochrome *a* is not observed, however, as the initial product of DMN reduction in the steady state because its reoxidation is much faster than the observed rate of electron donation that can be achieved from reduced DMN. A similar reactivity pattern is also observed when cytochrome bo_3 is reacted with reduced ubiquinone (*22*). In our case, an alternative explanation for the rapid appearance of reducing equivalents at cytochrome a_3 would propose direct electron transfer from menaquinol to the oxygen reaction site, bypassing cytochrome *a* as an intermediate carrier. If this

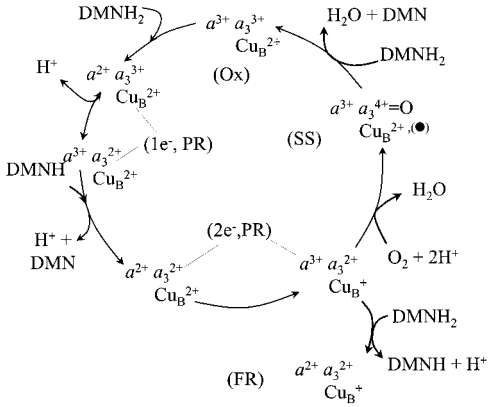

FIGURE 11: Kinetic scheme for partial reduction and catalytic cycle of cytochrome aa_3-600. Forms of the enzyme are indicated as (Ox) oxidized, (PR) partially reduced, (SS) steady state, and (FR) fully reduced.

were so, then the effect of cyanide binding in our transient reduction experiments would be to slow the initial rate of electron entry from menaquinol. However, cyanide binding to cytochrome a_3 enhances the initial rate of reduction. This result is consistent with cytochrome *a* as the initial electron acceptor from menaquinol, with the effect of cyanide being to slow the rate of cytochrome *a* reoxidation. The spectrum of reduced cytochrome *a* is observed in isolation, therefore, only when internal electron transfer is slow, as is achieved in the cyanide complex of the oxidized enzyme.

Following initial electron transfer from menaquinol to cytochrome *a*, cytochrome *a* reoxidation occurs via internal electron transfer (Figure 11) to again render cytochrome *a* available as an electron acceptor from reduced DMN. The product of the second reaction with reduced DMN promotes the enzyme to a two-electron reduced state, and it is now reactive with O_2. The products of the rapid, bimolecular reaction with O_2 at a rate of 5×10^7 M^{-1} s^{-1} (*8*) are a ferryl−oxo state of cytochrome a_3, oxidized Cu_B, a radical state of the enzyme, and 1 equiv of H_2O. The steady-state form of cytochrome aa_3-600 reacts again with reduced DMN to produce another equivalent of water and returns the enzyme to the oxidized state. The steady-state form of cytochrome aa_3-600 has the optical spectroscopic properties of the P intermediate as first defined with mammalian mitochondrial cytochrome *c* oxidase.

The P intermediate of mammalian cytochrome *c* oxidase was identified initially as a peroxy complex of cytochrome a_3 because it could be formed by the addition of peroxide to the oxidized enzyme (*23*). However, subsequent resonance Raman work demonstrated that the P-state was a ferryl−oxo form of cytochrome a_3 and that this species formed very early in the reaction with oxygen (*24*, *25*). Mass spectrometry studies of the P intermediate have confirmed that the dioxygen molecule is cleaved in this species and supports the assignment of a ferryl−oxo state to P (*26*). EPR studies of the P intermediate generated by adding peroxide to the oxidized enzyme reveal two different types of EPR signals that are assigned to either an amino acid based free radical or a porphyrin radical (*27*, *28*). Chemical modification of the P-state of bovine mitochondrial oxidase with excess halide traps an adduct of tyrosine 244 in subunit I that is generated via a radical state of the reactive tyrosine (*29*). Tyrosine 244 is part of a special structure in which the

tyrosine is covalently joined to histidine 240, which is a ligand to Cu_B (*30*−*32*). The characteristics of the radical signal reported here are consistent with its assignment to the homologous tyrosine in subunit I of cytochrome aa_3-600. However, we cannot rule out the possibility that the radical signal found here may arise from bound semiquinone that is a product of the one-electron reduction of oxidized enzyme. Our kinetic simulations do not predict appreciable accumulation of the semiquinone, but do predict the presence of the P-state to a level that is consistent with the magnitude observed for the free radical signal. A more certain assignment of this signal will require more detailed chemical and spectroscopic characterization, but our data do demonstrate the radical's participation in catalysis, and if the assignment to tyrosine is correct, it supports a redox role in catalysis for this structure as proposed by Babcock and co-workers (*29*).

Steady-state experiments on purified mitochondrial cytochrome *c* oxidase have characterized steady-state K_M values for the substrates cytochrome *c* and O_2 and maximal turnover values. Efforts to characterize the species of the enzyme that accumulates in the steady state have been hampered by heterogeneous behavior of the enzyme at the high concentrations required to observe the enzyme's spectral properties. For example, when reductants are added to isolated oxidized enzyme in detergent solution, the enzyme is initially hyperreduced and undergoes what is ascribed to a conformational change from a resting, less-active to a pulsed, more-reactive form (*17*). During this transition, the steady-state properties of the enzyme change. Measurements of single-turnover kinetics during the oxygen reaction of fully reduced enzyme have been used as the basis of proposed models of the catalytic cycle (e.g., *21*). If such a mechanism pertains under conditions used to observe the steady-state form of cytochrome *c* oxidase, then the presence of reduced cytochrome *a* should be minimal. However, in studies of isolated cytochrome *c* oxidase, substantial steady-state reduction of cytochrome *a* is observed (*17*). In the experiments reported here on cytochrome aa_3-600, reduced cytochrome *a* is not observed in the steady state. This implies that the cytochrome aa_3-600 complex does not undergo a slow activation when brought into the steady state, which is in contrast to what is observed with the bovine oxidase. In addition, the reoxidation of cytochrome *a* remains fast relative to electron input at all stages in the catalytic cycle of cytochrome aa_3-600. We suggest such behavior is more representative of the oxidase catalytic cycle in vivo and has been reported for the mammalian enzyme in situ in uncoupled rat liver mitochondria (*33*).

A feature of the reaction cycle shown here is that the fully oxidized, partially reduced, and P-state of the enzyme are participants in catalysis. Other states such as fully reduced and the F-state are not formally required in our model. In the case of the fully reduced state, it is clear that the enzyme does not achieve full reduction in the steady state. This is because of the rapid reaction of the two-electron-reduced enzyme with O_2, and its relatively slow reaction with reductant. The participation of the F-state is less clear. It may be that F-state occupancy is so low as to be below a detectable level, yet it may still be in the catalytic cycle.

We have provided for the first time spectroscopic evidence for the participation of a partially reduced O_2-bound intermediate as a player in the catalytic cycle of the heme−copper oxidase family. This has been suggested on numerous occasions, and preliminary evidence for a peroxy species during turnover of cytochrome bo_3 from *E. coli* has been reported (*34*). Whether P-species participation in catalysis is true for other members of this family of enzymes is something we will explore, as well as characterization of other members of the steady-state cycle. The enzyme under study here is a heme A-based menaquinol oxidase, and it has enough structural similarity to cytochrome *c* oxidase within its two largest and functionally relevant subunits to build a structural model. Whether this structural homology transfers into functional analogies such as modes of catalysis is a subject of active study.

REFERENCES

1. Musser, S. M., and Chan, S. I. (1998) *J. Mol. Evol. 46*, 508−520.
2. Michel, H., Behr, J., Harrenga, A., and Kannt, A. (1998) *Annu. Rev. Biophys. Biomol. Struct. 27*, 329−356.
3. Yoshikawa, S., Shinzawa-Itoh, K., and Tsukihara, T. (2000) *J. Inorg. Biochem. 82*, 1−7.
4. Lauraeus, M., Haltia, T., Saraste, M., and Wikström, M. (1991) *Eur. J. Biochem. 197*, 699−705.
5. Powers, L., Lauraeus, M., Reddy, K. S., Chance, B., and Wikström, M. (1994) *Biochim. Biophys. Acta 1183*, 504−512.
6. Fann, Y. C., Ahmed, I., Blackburn, N. J., Boswell, J. S., Verkhovskaya, M. L., Hoffman, B. M., and Wikström, M. (1995) *Biochemistry 34*, 10245−10255.
7. Hill, B. C., and Peterson, J. (1998) *Arch. Biochem. Biophys. 350*, 273−282.
8. Lauraeus, M., Morgan, J. E., and Wikström, M. (1993) *Biochemistry 32*, 2664−2670.
9. Hill, B. C. (1993) *Biochem. Biophys. Res. Commun. 192*, 665−670.
10. Lemma, E., Schagger, H., and Kröger, A. (1993) *Arch. Microbiol. 159*, 574−578.
11. Lemma, E., Simon, J., Schagger, H., and Kröger, A. (1995) *Arch. Microbiol. 163*, 432−438.
12. Hill, B. C. (1994) *J. Biol. Chem. 269*, 2419−2425.
13. Henning, W., Vo, L., Albanese, J., and Hill, B. C. (1995) *Biochem. J. 309*, 279−283.
14. Wrigglesworth, J. M., Ioannidis, N., and Nicholls, P. (1988) *Ann. N.Y. Acad. Sci. 550*, 150−160.
15. Verkhovsky, M. I., Morgan, J. E., and Wikström, M. (1995) *Biochemistry 34*, 7483−7491.
16. Chen, S., Knox, R., Wu, K., Deng, P. S., Zhou, D., Bianchet, M. A., and Amzel, L. M. (1997) *J. Biol. Chem. 272*, 1437−1439.
17. Nicholls, P., Hildebrandt, V., Hill, B. C., Nicholls, F., and Wrigglesworth, J. M. (1980) *Can. J. Biochem. 58*, 969−977.
18. Wikström, M., and Morgan, J. E. (1992) *J. Biol. Chem. 267*, 10266−10273.
19. Proshlyakov, D. A., Pressler, M. A., and Babcock, G. T. (1998) *Proc. Natl. Acad. Sci. U.S.A. 95*, 8020−8025.
20. Szundi, I., Liao, G. L., and Einarsdottir, O. (2001) *Biochemistry 40*, 2332−2339.
21. Babcock, G. T. (1999) *Proc. Natl. Acad. Sci. U.S.A. 96*, 12971−12973.
22. Schultz, B. E., Edmondson, D. E., and Chan, S. I. (1998) *Biochemistry 37*, 4160−4168.
23. Bickar, D., Bonaventura, J., and Bonaventura, C. (1982) *Biochemistry 21*, 2661−2666.
24. Kitagawa, T. (2000) *J. Inorg. Biochem. 82*, 9−18.
25. Han, S., Takahashi, S., and Rousseau, D. L. (2000) *J. Biol. Chem. 275*, 1910−1919.
26. Fabian, M., Wong, W. W., Gennis, R. B., and Palmer, G. (1999) *Proc. Natl. Acad. Sci. U.S.A. 96*, 13114−13117.
27. Rigby, S. E., Junemann, S., Rich, P. R., and Heathcote, P. (2000) *Biochemistry 39*, 5921−5928.

28. MacMillan, F., Kannt, A., Behr, J., Prisner, T., and Michel, H. (1999) *Biochemistry 38*, 9179−9184.
29. Proshlyakov, D. A., Pressler, M. A., DeMaso, C., Leykam, J. F., DeWitt, D. L., and Babcock, G. T. (2000) *Science 290*, 1588−1591.
30. Ostermeier, C., Harrenga, A., Ermler, U., and Michel, H. (1997) *Proc. Natl. Acad. Sci. U.S.A. 94*, 10547−10553.
31. Yoshikawa, S., Shinzawa-Itoh, K., Nakashima, R., Yaono, R., Yamashita, E., Inoue, N., Yao, M., Fei, M. J., Libeu, C. P., Mizushima, T., Yamaguchi, H., Tomizaki, T., and Tsukihara, T. (1998) *Science 280*, 1723−1729.
32. Buse, G., Soulimane, T., Dewor, M., Meyer, H. E., and Bluggel, M. (1999) *Protein Sci. 8*, 985−990.
33. Morgan, J. E., and Wikström, M. (1991) *Biochemistry 30*, 948−958.
34. Moody, A. J., Rumbley, J. N., Ingledew, W. J., Gennis, R. B., and Rich, P. R. (1993) *Biochem. Soc. Trans. 21*, 255S.

BI011116Q